

Sparsely Activated Networks

Paschalis Bizopoulos, and Dimitrios Koutsouris

Abstract—Previous literature on unsupervised learning focused on designing structural priors and optimization functions with the aim of learning meaningful features, but without considering the description length of the representations. Here we present Sparsely Activated Networks (SANs), which decompose their input as a sum of sparsely reoccurring patterns of varying amplitude, and combined with a newly proposed metric φ they learn representations with minimal description lengths. SANs consist of kernels with shared weights that during encoding are convolved with the input and then passed through a ReLU and a sparse activation function. During decoding, the same weights are convolved with the sparse activation map and the individual reconstructions from each weight are summed to reconstruct the input. We also propose a metric φ for model selection that favors models which combine high compression ratio and low reconstruction error and we justify its definition by exploring the hyperparameter space of SANs. We compare four sparse activation functions (Identity, Max-Activations, Max-Pool indices, Peaks) on a variety of datasets and show that SANs learn interpretable kernels that combined with φ , they minimize the description length of the representations.

Index Terms—artificial neural networks, autoencoders, compression, sparsity

I. INTRODUCTION

Deep Neural Networks (DNNs) [1] is a class of representation learning models, which make use of multiple stacked layers containing weights and activation functions that transform the input to intermediate representations during the feed-forward pass. Using backpropagation [2] the gradient of each weight w.r.t. the error of the output is efficiently calculated and passed to an optimization function such as Stochastic Gradient Descent or Adam [3] which updates the weights making the output of the network converge to the desired output. DNNs have been successful in utilizing big data and powerful parallel processing units and have achieved state-of-the-art performance in problems such as image [4] and speech recognition [5]. However, these breakthroughs have come at the expense of increased description length of the learned representations, which in DNNs is proportional with the number of:

- 1) weights of the model and
- 2) non-zero activations.

The use of large number of weights as a design choice in architectures such as Inception [6], VGGnet [7] and ResNet [8] (usually by increasing the depth) was followed by research that signified the weight redundancy of DNNs. It was demonstrated that DNNs easily fit random labeling of the data [9] and that in any initialized DNN there exists a subnetwork that can solve

the given problem with the same accuracy with the originally trained one [10].

Moreover, DNNs with large number of weights have higher storage requirements and they are slower during inference. Previous literature addressing this problem has focused on weight pruning from trained DNNs [11] and weight pruning during training [12], with the aim to minimize the model capacity for use in environments with low computational capabilities, or low inference time requirements. Pruning strategies however, only take in consideration the model capacity and only indirectly the description length of the representation.

The other element that affects the description length of the representation of DNNs is, the number of non-zero activations in the intermediate representations which is related with the concept of activity sparseness. Sparseness can be applied in neural networks either in the connections between neurons, or in the activation maps [13]. Although sparseness in the activation maps is usually enforced in the loss function by adding a $L_{1,2}$ regularization or Kullback-Leibler divergence term [14], we could also achieve sparsity in the activation maps with the use of an appropriate activation function.

Initially, bounded functions such as sigmoid and tanh were used, however besides producing dense activation maps they also present the vanishing gradients problem [15]. Rectified Linear Units (ReLU) were later proposed [16], [17] as an activation function that solves the vanishing gradients problem and increases the sparsity of the activation maps. Although ReLU creates exact zeros (unlike its predecessors sigmoid and tanh), its activation map consists of sparsely separated but still dense areas (Fig. 1(a)) instead of sparse spikes. The same applies for other generalizations of ReLU, such as Parametric ReLU [18] and Maxout [19]. Recently, in k -Sparse Autoencoders [20] the authors used an activation function that applies thresholding until the k most active activations remain, however this non-linearity covers a limited area of the activation map by creating sparsely disconnected dense areas (Fig. 1(b)), similar to the ReLU case.

Activation functions that produce continuous valued activation maps are less biologically plausible, because biological neurons rarely are in their maximum saturation regime [21] and use spikes to communicate instead of continuous values [22]. Previous literature has also demonstrated the increased biological plausibility of sparseness in artificial neural networks [23]. Spike-like sparsity on activation maps has been thoroughly researched on the more biologically plausible rate-based network models [24], but it has not been thoroughly explored as a design option for activation functions combined with convolutional filters.

The increased number of weights and non-zero activations make DNNs more complex, and thus they are more difficult for use in problems that require corresponding causality of

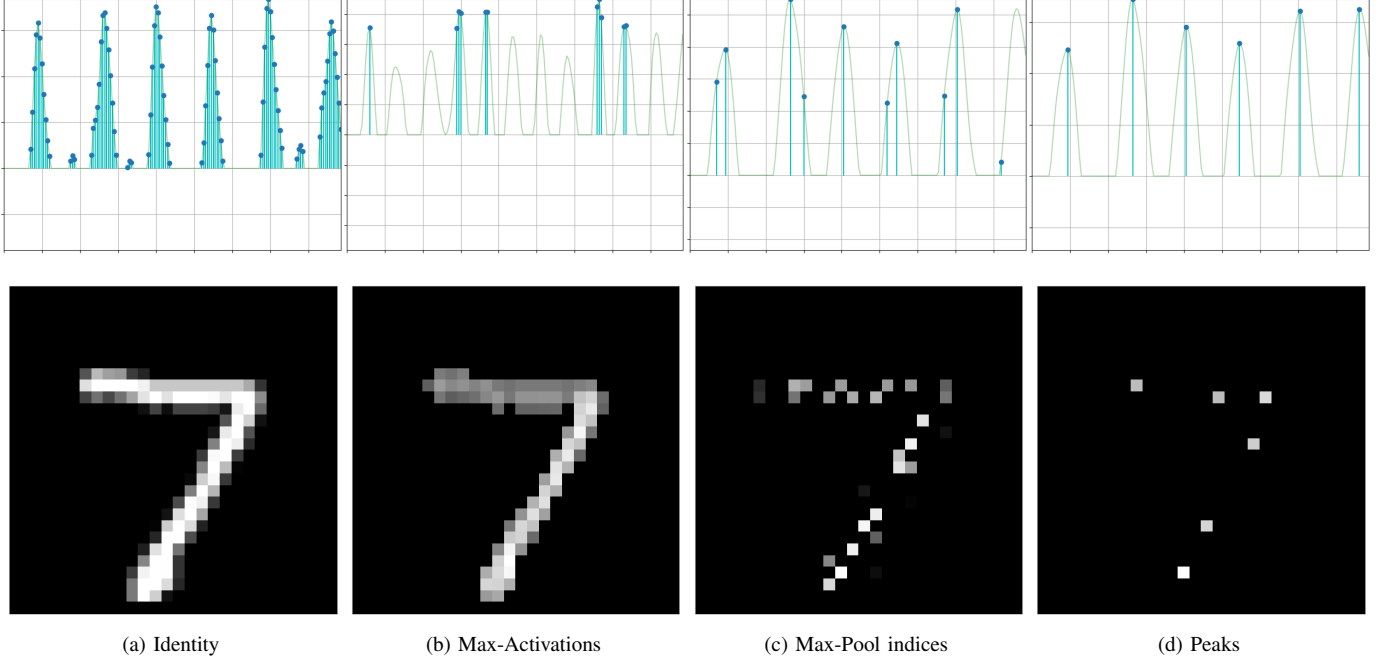


Fig. 1. Visualization of four sparse activation functions (Identity, Max-Activations, Max-Pool indices and Peaks) for 1D and 2D input in the first and second row respectively. The 1D input to the activation functions is denoted with the continuous transparent green line and consists of an example from the UCI dataset. The output of each activation function is denoted with the cyan stem lines with blue markers. The 2D example depicts only the output of the activation functions using an example from the MNIST dataset.

the output with a specific set of neurons. Many critical areas such as healthcare [25] require models to be interpretable and explainable before considering them as a solution. Although these properties can be increased using sensitivity analysis [26], deconvolution methods [27], Layerwise-Relevance Propagation [28] and Local-Interpretable Model agnostic Explanations [29] it would be preferable to have self-interpretable models.

Moreover, considering that DNNs learn to represent (or equivalently compress) data using the combined set of trainable weights (i.e. model capacity) and non-zero activations during the feed-forward pass, an interesting question arises:

What are the implications of trading off the reconstruction error of the representations with their compression ratio w.r.t to the original data?

Previous work by Blier et al. [30] demonstrated the ability of DNNs to losslessly compress the input data and the weights, but without considering non-zero activations. In this work we relax the lossless requirement and also consider neural networks purely as function approximators instead of probabilist models. The contributions of this paper are the following proposals:

- Sparsely Activated Networks (SANs) (Fig. 2) in which spike-like sparsity is enforced in the activation map through a sparse activation function (Fig. 1(c) and (d)).
- a model selection metric φ that favors models which combine small number of weights and non-zero activations w.r.t to the original size of the data and low

reconstruction error. By exploring the hyperparameter space of the kernel sizes of SANs we also justify the definition of φ as a metric.

In section II we define the architecture and training of SANs along with the four tested sparse activation functions, in section III we define the φ metric, in section IV we experiment SANs on the Physionet, UCI-epilepsy and MNIST databases and provide visualizations of the intermediate representations and results. In section V we discuss the findings of the experiments and the limitations of SANs and finally in section VI we present the concluding remarks and the future work.

II. SPARSELY ACTIVATED NETWORKS

In the following subsections we will define the architecture and training of SANs and then the four sparse activation functions that we later compare during the experiments.

A. SAN Architecture/Training

Let $\mathbf{x} \in \mathbb{R}^n$ be one input data, however the following can be trivially generalized to batch inputs with different cardinalities. Let $\mathbf{w}^{(i)} \in \mathbb{R}^{m^{(i)}}$ the weight matrix of the i^{th} kernel, that are initialized using a normal distribution with mean μ and standard deviation σ :

$$\mathbf{w}^{(i)} \sim \mathcal{N}(\mu, \sigma) \quad (1)$$

, where $0 \leq i < q \in \mathbb{N}$ is the number of kernels.

First we calculate the similarity matrices¹ $\mathbf{s}^{(i)}$ for each of the weight matrices $\mathbf{w}^{(i)}$:

$$\mathbf{s}^{(i)} = \mathbf{x} * \mathbf{w}^{(i)} \quad (2)$$

¹Previous literature refers to this as the ‘hidden variable’ but we use a more direct name that suits the context of this paper.

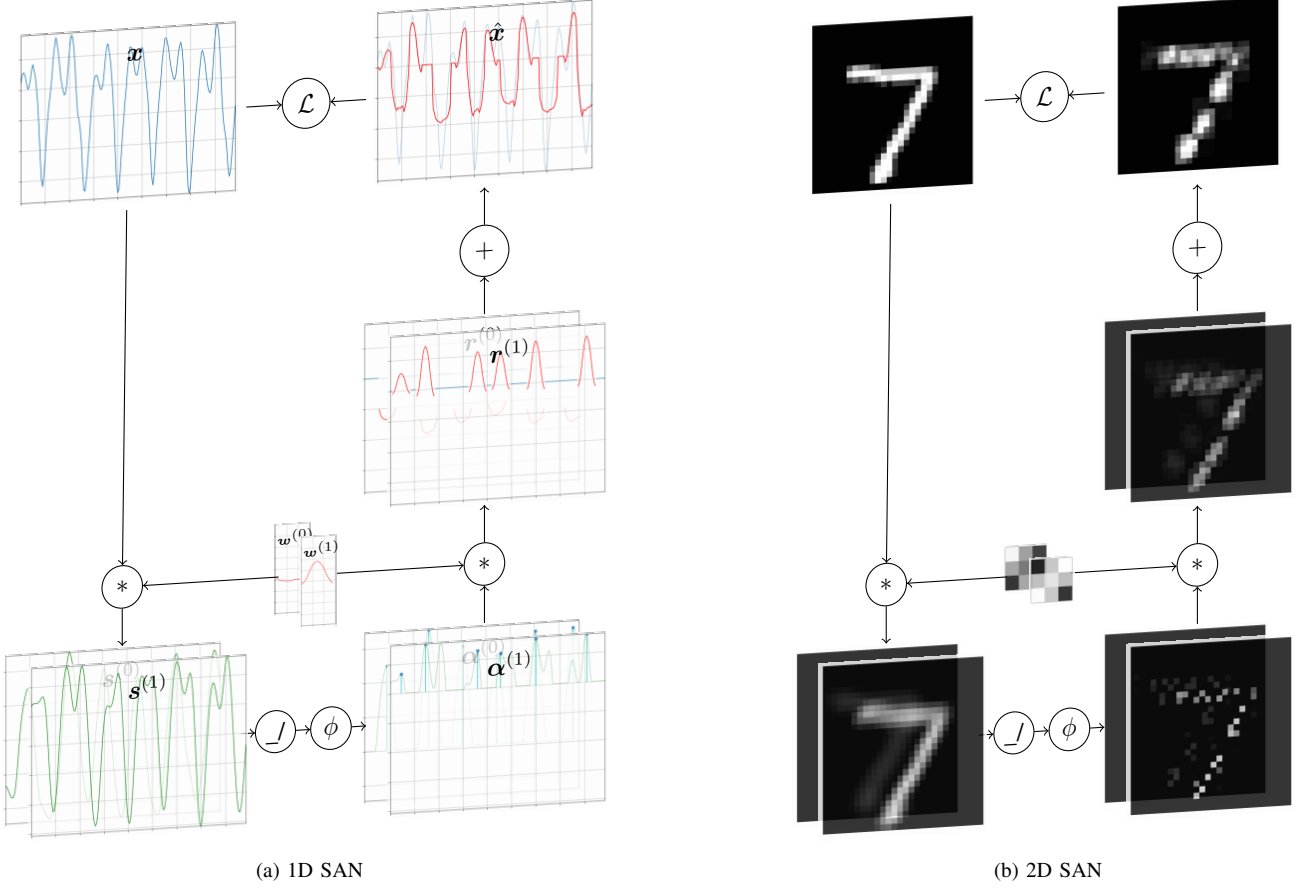


Fig. 2. Diagrams of the feed-forward pass of 1D and 2D SANs with two kernels for random examples from the test dataset of UCI epilepsy database and MNIST respectively. The figures depict intermediate representations; \mathbf{x} denotes the input signal (blue line), $\mathbf{w}^{(i)}$ denotes the kernels (red line), $\mathbf{s}^{(i)}$ denotes the similarity matrices (green line), $\alpha^{(i)}$ denotes the peak matrices (cyan stem lines with blue markers), $\mathbf{r}^{(i)}$ denotes the individual reconstruction from each $\mathbf{w}^{(i)}$ and $\hat{\mathbf{x}}$ denotes the reconstructed input (red line). Placed for comparison, the transparent green line in $\alpha^{(i)}$ denotes the corresponding $\mathbf{s}^{(i)}$ and the transparent blue line in $\hat{\mathbf{x}}$ denotes the input \mathbf{x} . The exponent $i = 0, 1$ corresponds to the first and second kernel and corresponding intermediate representations respectively. The circles denote operations; \mathcal{L} denotes the loss function, \mathcal{J} denotes the ReLU activation function, ϕ denotes the sparse activation function, $*$ the convolution operation and $+$ the plus operator. All operations are performed separate for each $\mathbf{w}^{(i)}$ however for visual clarity we only depict one operation for each step. The Peak sparse activation was used for the 1D example and the Max-Pool indices for the 2D.

, where $*$ is the convolution² operation with ‘same padding’. We do not need a bias term because it would be applied globally on $\mathbf{s}^{(i)}$ which is almost equivalent with learning the baseline of \mathbf{x} .

We then pass $\mathbf{s}^{(i)}$ through a ReLU activation function which results in:

$$\mathbf{s}_{ReLU}^{(i)} = ReLU(\mathbf{s}^{(i)}) \quad (3)$$

We apply ReLU on $\mathbf{s}^{(i)}$ to keep only the positive similarities of the matrix because activations with negative amplitude do not necessarily have proportional negative similarity with $\mathbf{w}^{(i)}$. However, a direct utilization of the negative side of the $\mathbf{s}^{(i)}$ would be to detect local valleys (instead of peaks) activations with the negative amplitude, using the negative correlation of this region with $\mathbf{w}^{(i)}$.

²We use convolution instead of cross-correlation only as a matter of compatibility with previous literature and computational frameworks. Using cross-correlation would produce the same results and would not require flipping the kernels during visualization.

We then pass $\mathbf{s}_{ReLU}^{(i)}$ and a sparsity parameter $d^{(i)}$ in the sparse activation function ϕ resulting in the activation map $\alpha^{(i)}$:

$$\alpha^{(i)} = \phi(\mathbf{s}_{ReLU}^{(i)}, d^{(i)}) \quad (4)$$

, where $\alpha^{(i)}$ is a sparse matrix that its non-zero elements denote the spatial positions of the instances of the i^{th} kernel. The form of ϕ and $d^{(i)}$ depend on the choice of the sparse activation function which are presented in section II-B.

We convolve each $\alpha^{(i)}$ with its corresponding $\mathbf{w}^{(i)}$ resulting in a set of individual reconstructions $\mathbf{r}^{(i)}$ of the input:

$$\mathbf{r}^{(i)} = \alpha^{(i)} * \mathbf{w}^{(i)} \quad (5)$$

, which consists of sparsely reoccurring patterns of $\mathbf{w}^{(i)}$ with variable amplitude. Finally we can reconstruct the input as the sum of the individual reconstructions $\mathbf{r}^{(i)}$ as follows:

$$\hat{\mathbf{x}} = \sum_{i=1}^q \mathbf{r}^{(i)} \quad (6)$$

The Mean Absolute Error (MAE) of the input \mathbf{x} and the prediction $\hat{\mathbf{x}}$ is then calculated using the following:

$$\mathcal{L}(\mathbf{x}, \hat{\mathbf{x}}) = \frac{1}{n} \sum_{t=1}^n |\hat{\mathbf{x}}_t - \mathbf{x}_t| \quad (7)$$

, where the index t denotes the t^{th} sample. The choice of MAE is based on the need to handle outliers in the data with the same weight as normal values. However, SANs are not restricted in using MAE and other loss functions could be used, such as Mean Square Error.

Using backpropagation, the gradients of the loss \mathcal{L} w.r.t the $\mathbf{w}^{(i)}$ are calculated:

$$\nabla \mathcal{L} = \left(\frac{\partial \mathcal{L}}{\partial \mathbf{w}^{(1)}}, \dots, \frac{\partial \mathcal{L}}{\partial \mathbf{w}^{(q)}} \right) \quad (8)$$

Lastly the $\mathbf{w}^{(i)}$ are updated using the following learning rule:

$$\Delta \mathbf{w}^{(i)} = -\lambda \frac{\partial \mathcal{L}}{\partial \mathbf{w}^{(i)}} \quad (9)$$

, where λ is the learning rate.

After training, we consider $\alpha^{(i)}$ (which is calculated during the feed-forward pass from Eq. 4) and $\mathbf{w}^{(i)}$ (which is calculated using backpropagation from Eq. 9) the compressed representation of \mathbf{x} , which can be reconstructed using Equations 5 and 6:

$$\hat{\mathbf{x}} = \sum_{i=1}^q \left(\alpha^{(i)} * \mathbf{w}^{(i)} \right) \quad (10)$$

The training of SANs for multiple epochs using batches (instead of one example as previously shown) is presented in Algorithm 1.

Algorithm 1 Sparsely Activated Networks training

Input: \mathbf{x}

Output: α, \mathbf{w}

Hyperparameters: $m, \mu, \sigma, q, \phi, d, \lambda, \text{epochs}, \text{batches}$

```

1: for  $i = 1$  to  $q$  do
2:    $\mathbf{w}^{(i)} \sim \mathcal{N}(\mu, \sigma)$ 
3: end for
4: for  $e = 1$  to  $\text{epochs}$  do
5:   for  $b = 1$  to  $\text{batches}$  do
6:      $\mathbf{x}^{(b)} \sim \mathbf{x}$ 
7:     for  $i = 1$  to  $q$  do
8:        $\mathbf{s}^{(i)} \leftarrow \mathbf{x}^{(b)} * \mathbf{w}^{(i)}$ 
9:        $\alpha^{(i)} \leftarrow \phi(\mathbf{s}^{(i)}, d^{(i)})$ 
10:       $\mathbf{r}^{(i)} \leftarrow \alpha^{(i)} * \mathbf{w}^{(i)}$ 
11:    end for
12:     $\hat{\mathbf{x}}^{(b)} \leftarrow \sum_{i=1}^q \mathbf{r}^{(i)}$ 
13:     $\mathcal{L} \leftarrow \frac{1}{n} \sum_{t=1}^n |\hat{\mathbf{x}}_t^{(b)} - \mathbf{x}_t^{(b)}|$ 
14:     $\nabla \mathcal{L} = \left( \frac{\partial \mathcal{L}}{\partial \mathbf{w}^{(1)}}, \dots, \frac{\partial \mathcal{L}}{\partial \mathbf{w}^{(q)}} \right)$ 
15:     $\Delta \mathbf{w}^{(i)} = -\lambda \frac{\partial \mathcal{L}}{\partial \mathbf{w}^{(i)}}$ 
16:  end for
17: end for
18: return  $\alpha, \mathbf{w}$ 
```

B. Sparse Activation Functions

In this subsection we define four sparse activation functions ϕ . Identity and Max-Activation convert their input to sparsely disconnected but internally dense areas, while Max-Pool indices and Peaks convert their input to spike-like sparse activation maps according to a sparsity parameter $d^{(i)}$. We choose specific values for $d^{(i)}$ for each sparse activation function in such a way, to approximately have the same number of activations for fair comparison of the sparse activation functions (besides the Identity).

1) *Identity*: $\phi = \mathbb{1}$. The Identity activation function serves as a baseline and combined with the previously applied ReLU on $\mathbf{s}^{(i)}$ it produces sparsely disconnected dense areas as shown in Fig. 1(a) instead of sparse spikes. For this case $d^{(i)}$ does not apply.

2) *Max-Activations*: The Max-Activation function (defined at Algorithm 2) keeps the k largest activations and zeros out the rest, where $1 \leq k < n \in \mathbb{N}$. We set $d^{(i)} = k$, where $k = \lfloor n/m \rfloor^{\dim(\mathbf{x})}$ and \dim denotes dimensionality.

Algorithm 2 Max-Activations

Input: s, k

Output: u

```

1:  $u_i \leftarrow 0, i = 1 \dots |s|$ 
2:  $p \leftarrow \text{topk}(s, k)$ 
3: for  $i = 0$  to  $|s|$  do
4:    $u_i(p_i) = s_i(p_i)$ 
5: end for
6: return  $u$ 
```

3) *Max-Pool indices*: The Max-Pool indices activation function (defined at Algorithm 3) keeps only the max activation from each region outlined by a grid as granular as the kernel size $m^{(i)}$ and zeros out the rest. It consists of a max-pooling layer followed by a max-unpooling layer with the same parameters while the sparsity parameter $d^{(i)}$ in this case is set $d^{(i)} = m^{(i)} < n \in \mathbb{N}$.

Algorithm 3 Max-Pool indices

Input: s, m

Output: u

```

1:  $p \leftarrow \text{maxpool}(s, m)$ 
2:  $u \leftarrow \text{maxunpool}(s(p), p, m)$ 
3: return  $u$ 
```

4) *Peaks*: The Peaks activation function (defined at Algorithm 4) detects candidate peaks using zero crossing of the first derivative, then sorts them in an descending order and gradually eliminates those peaks that have less amplitude than a neighboring peak within a predefined distance mpd . Imposing a minimum peak distance on the peak detection algorithm makes α more sparse than the previous cases. The sparsity parameter in this case is set $d^{(i)} = mpd$, where $1 \leq mpd < n \in \mathbb{N}$ is the minimum peak distance. We set $mpd = m^{(i)}$ for utilizing fair comparison between the sparse activation functions.

Algorithm 4 Peak detection with minimum peak distance mpd **Input:** s, mpd **Output:** u

```

1:  $z \leftarrow \frac{ds}{dt} > 0 \wedge \frac{ds}{dt} < 0$ 
2:  $p_i \leftarrow z > 0$ 
3:  $p_{i_i} \leftarrow \text{sort}(z)$ 
4:  $p_{i_{sorted}} \leftarrow p_i(p_{i_i})$ 
5:  $q_i \leftarrow 0, i = 1 \dots |s|$ 
6: for  $i = 0$  to  $|s|$  do
7:   if  $\neg q_i$  then
8:      $p_{i_r} \leftarrow p_i \geq p_{i_i} - mpd$ 
9:      $p_{i_l} \leftarrow p_i \leq p_{i_i} + mpd$ 
10:     $p_{i_m} \leftarrow p_{i_r} \wedge p_{i_l}$ 
11:     $q \leftarrow q \vee p_{i_m}$ 
12:     $q_i \leftarrow 0$ 
13:   end if
14: end for
15:  $u_{ind} \leftarrow p_{i_{sorted}}(\neg q)$ 
16:  $u_i \leftarrow 0, i = 1 \dots |s|$ 
17:  $u(u_i) \leftarrow s(u_{ind})$ 
18: return  $u$ 

```

III. φ METRIC

From a high level point of view, the evaluation of SANs will be done on two axis: their verbosity and their accuracy. More precisely, considering Eq. 10 our target is to estimate an as accurate as possible representation of \mathbf{x} through $\alpha^{(i)}$ and $\mathbf{w}^{(i)}$ with the least amount of number of non-zero activations and weights.

Verbosity in neural networks can be perceived as inversely proportional to the compression ratio of the representations. First, we define the number of weights W of a model M as follows:

$$W = \sum_{i=1}^q m^{(i)} \quad (11)$$

, where q and $m^{(i)}$ were previously defined as the number of kernels and the cardinality of the i^{th} kernel respectively.

We also define the number of non-zero activations A of \mathbf{x} of a model M as:

$$A_{\mathbf{x}} = \sum_{i=1}^q \|\alpha^{(i)}\|_0 \quad (12)$$

, where $\|\cdot\|_0$ denotes the ℓ_0 pseudo-norm. Then using Equations 11 and 12 we define the compression ratio CR of \mathbf{x} w.r.t M as:

$$CR = \frac{n}{W + (\dim(\mathbf{x}) + 1)A_{\mathbf{x}}} \quad (13)$$

The reason that we multiply the dimensionality of \mathbf{x} with the number of activations $A_{\mathbf{x}}$ is that we need to consider the spatial position of each non-zero activation in addition to its amplitude to reconstruct \mathbf{x} . Moreover, using that definition of CR , there is a desirable trade-off between using a larger kernel with less instances and a smaller kernel with more instances based on which kernel size minimizes the CR .

Regarding the accuracy, we define the normalized reconstruction loss as follows:

$$\tilde{\mathcal{L}}(\hat{\mathbf{x}}, \mathbf{x}) = \frac{\mathcal{L}(\hat{\mathbf{x}}, \mathbf{x})}{\mathcal{L}(0, \mathbf{x})} \quad (14)$$

Finally using Equations 13 and 14 we define the φ^3 metric of \mathbf{x} w.r.t M as follows:

$$\varphi = \frac{1}{2} \left(CR^{-1} + \tilde{\mathcal{L}}(\hat{\mathbf{x}}, \mathbf{x}) \right) \quad (15)$$

, where the $1/2$ factor is used to keep φ in the range $[0, 1]$, since CR^{-1} and $\tilde{\mathcal{L}}$ are already within this range, however they might take values outside of this range.

Regarding hyperparameter selection we also define the mean φ of a dataset or a mini-batch w.r.t to M as:

$$\bar{\varphi} = \frac{1}{l} \sum_{j=1}^l \varphi^{(j)} \quad (16)$$

, where l is the number of observations in the dataset or the batch size.

$\bar{\varphi}$ is non-differentiable due to the presence of the ℓ_0 pseudo-norm in Eq. 12. A way to overcome this is using \mathcal{L} as the differentiable optimization function during training and $\bar{\varphi}$ as the metric for model selection during validation on which hyperparameter value decisions (such as kernel size) are made.

IV. EXPERIMENTS

For all experiments the weights of the SAN kernels are initialized using the normal distribution $\mathcal{N}(\mu, \sigma)$ with $\mu = 0$ and $\sigma = 0.1$. We used Adam [3] as the optimizer with learning rate $\lambda = 0.01$, $b_1 = 0.9$, $b_2 = 0.999$, epsilon $\epsilon = 10^{-8}$ without weight decay. For implementing and training SANs we used Pytorch [31] with a NVIDIA Titan X Pascal GPU 12GB RAM and a 12 Core Intel i7-8700 CPU @ 3.20GHz on a Linux operating system.

A. Comparison of $\bar{\varphi}$ for sparse activation functions and various kernel sizes in Physionet

We study the effect on $\bar{\varphi}$, of the combined choice of the kernel size m and the sparse activation functions that were defined in section II-B.

1) *Datasets*: We use one signal from each of 15 signal datasets from Physionet [32] listed in the first column of Table I. Each signal consists of 12000 samples which in turn is split in 12 signals of 1000 samples each, to create the training (6 signals), validation (2 signals) and test datasets (4 signals). The only preprocessing that is done is mean subtraction and division of one standard deviation on the 1000 samples signals.

³The use of the symbol φ comes from the first character of the combined greek noun $\varphi\lambda\epsilon\theta\omicron\varsigma$ = $\varphi\lambda\epsilon\theta\omicron\varsigma + \theta\varsigma$ (flethos: pronounced as flee-thos). It consists of the first part of the word $\varphi\lambda\epsilon\theta\omicron\varsigma$ - $\theta\varsigma$ (meaning verbose) and the second part of $\varphi\lambda\epsilon\theta\omicron\varsigma$ - $\theta\varsigma$ (meaning wrong). $\varphi\lambda\epsilon\theta\omicron\varsigma$ is literally defined as: *Giving inaccurate information using many words; the state of being wrong and wordy at the same time.*

2) *Experiment Setup*: We train four SANs (one for each sparse activation function) for each of the 15 Physionet datasets, for 20 epochs with a batch size of 2 with one kernel of varying size in the range $[1, 250]$. During validation we selected the models with the kernel size that achieved the best $\bar{\varphi}$ out of all epochs. During testing we feed the test data into the selected model and calculate CR^{-1} , $\hat{\mathcal{L}}$ and $\bar{\varphi}$ for this set of hyperparameters as shown in Table I.

3) *Results*: The two separate clusters which are depicted in Fig. 3 between the Identity activation function and the rest the effect of a sparser activation function on the representation. The sparser an activation function is the more it compresses, sometimes at the expense of reconstruction error. However, by visual inspection of Fig. 5 one could confirm that the learned weights of the SAN with sparser activation maps (Max-Pool indices and Peaks) correspond to the reoccurring patterns in the datasets, thus having high interpretability. These results suggest that reconstruction error by itself is not a sufficient metric for decomposing data in interpretable components. Trying to solely achieve lower reconstruction error (such as the case for the Identity activation function) produces noisy learned kernels, while the combined measure of reconstruction error and compression ratio (smaller $\bar{\varphi}$) demonstrates interpretable kernels. Comparing the differences of $\bar{\varphi}$ between the Identity and the rest sparse activation functions in Fig. 4 we notice that the latter have a less noisy $\bar{\varphi}$ when m is varied and second, although they generally increase, they produce a minimum region in which we observe interpretable kernels (as shown in the plots with the yellow background in Fig. 3).

B. Evaluation of the reconstruction of SANs using a Supervised CNN on UCI-epilepsy

We study the quality of the reconstructions of SANs by training a supervised 1D Convolutional Neural Network (CNN) on the output of each SAN. We also study the effect that m has on $\bar{\varphi}$ and the accuracy of the classifier for the four sparse activation functions.

1) *Dataset*: We use the UCI-epilepsy recognition dataset [33] that consists of 500 signals each one with 4097 samples (23.5 seconds). The dataset is annotated into five classes with 100 signals for each class. For the purposes of this paper we use a variation of the database⁴ in which the EEG signals are split into segments with 178 samples each, resulting in a balanced dataset that consists of 11500 EEG signals in total.

2) *Experiment Setup*: First, we merge the tumor classes (2 and 3) and the eyes classes (4 and 5) resulting in a modified dataset of three classes (tumor, eyes, epilepsy). We then split the 11500 signals into 76%, 12% and 12% (8740, 1380, 1380 signals) as training, validation and test data respectively and normalize in the range $[0, 1]$ using the global max and min. For the SANs, we used two kernels $q = 2$ and trained for 20 epochs with a batch size of 16. After training, we choose the model that performed the lowest $\bar{\varphi}$ out of all epochs.

During supervised learning the weights of the kernels are frozen and a CNN is stacked on top of the final reconstructions

of the SANs. The CNN feature extractor consists of two convolutional layers with 3 and 16 filters and kernel size 5, each one followed by a ReLU and a Max-Pool with pool size 2. The classifier consists of three fully connected layers with 656, 120 and 84 units. The first two fully connected layers are followed by a ReLU while the last one is passed through a log-softmax that produces the predictions. The CNN is trained for an additional 20 epochs with the same batch size and the model selection procedure as with SANs and Negative Log-Likelihood as the loss function.

3) *Results*: As shown in Table. II, although we use a significantly reduced representation size, the accuracies do not drop proportionally which suggests that SANs choose the most important features to represent the data. For example for $m = 15$ for the Peak activation function, there is a drop in accuracy of 15.84% (the baseline CNN on the original data achieved 90.54%) although a reduced representation is used with only 26% of the size w.r.t the original data.

C. Evaluation of the reconstruction of SANs using a Supervised FNN on MNIST

1) *Dataset*: For the same task as the previous one but for 2D, we use MNIST [34] which consists of a training dataset of 60000 greyscale images with handwritten digits and a test dataset of 10000 images each one having size of 28×28 .

2) *Experiment Setup*: The models consist of two kernels $q = 2$ for which their size ranges from 1 to 7. We use 10000 images from the training dataset as a validation dataset and train on the rest 50000 for 20 epochs with a batch size of 64. We do not apply any preprocessing on the images.

During supervised learning the weights of the kernels are frozen and a one layer fully connected network (FNN) is stacked on top of the final reconstructions of the SANs. The FNN is trained for an additional 20 epochs with the same batch size and model selection procedure as with SANs and Negative Log-Likelihood as the loss function.

3) *Results*: As shown in Table. III the accuracies achieved by the reconstructions of some SANs are comparable to those of an FNN trained on the original data (91.53%), although they have been heavily compressed. It is interesting to note that in some cases SANs reconstructions, such as for the Max-Pool indices, performed even better than the original data. This suggests the overwhelming presence of redundant information that resides in the raw pixels of the original data.

V. DISCUSSION

SANs combined with the φ metric compress the description of the data in a way a minimum description language framework would, by encoding them into $w^{(i)}$ and $\alpha^{(i)}$.

From the point of view of Sparse Dictionary Learning, SANs kernels could be seen as the atoms of a learned dictionary specializing in interpretable pattern matching (e.g. for ECG input the kernels of SANs are ECG beats) and the sparse activation map as the representation. The fact that SANs are wide with fewer larger kernel sizes instead of deep with smaller kernel sizes make them more interpretable than

⁴<https://archive.ics.uci.edu/ml/datasets/Epileptic+Seizure+Recognition>

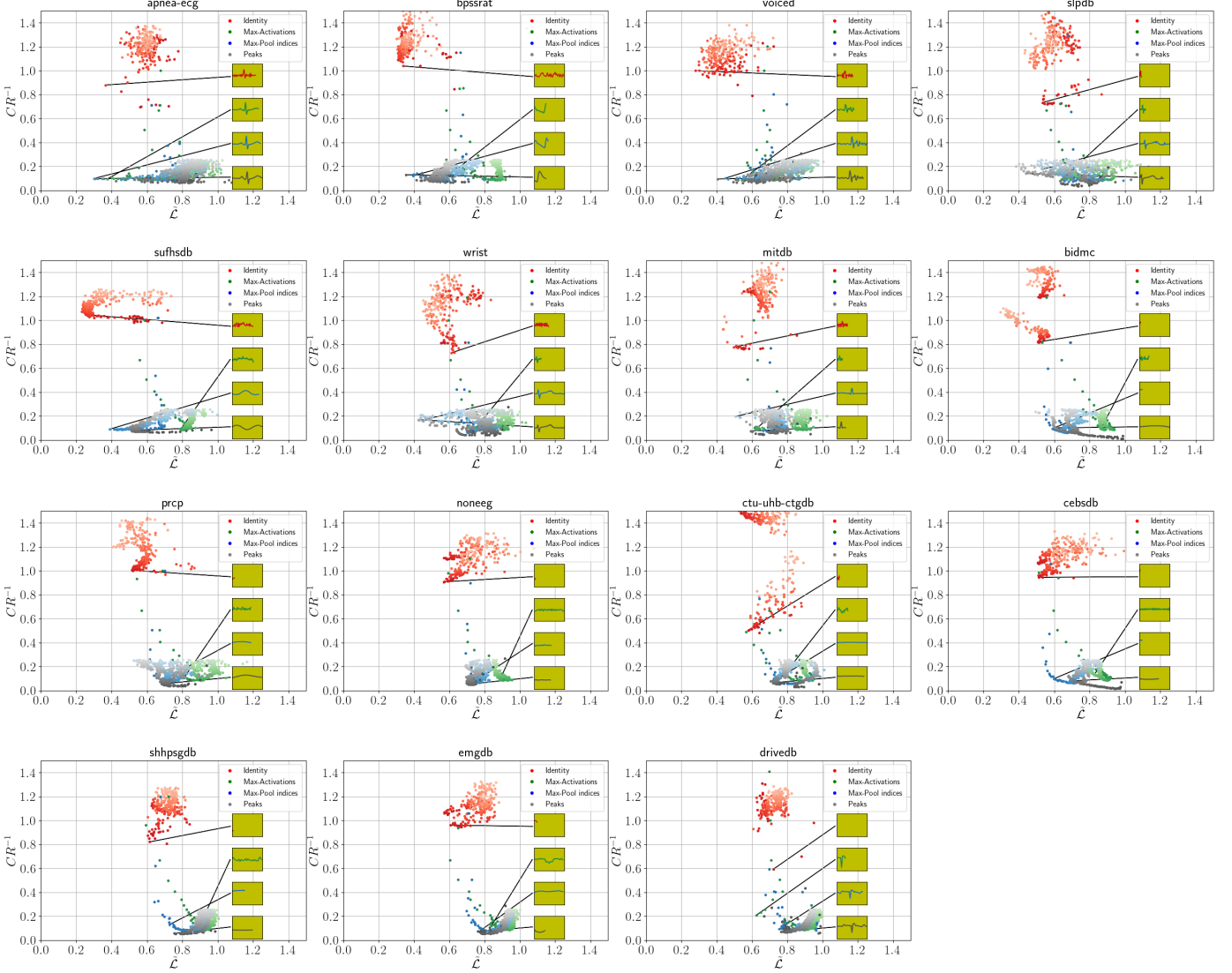


Fig. 3. Inverse compression ratio (CR^{-1}) vs. normalized reconstruction loss ($\tilde{\mathcal{L}}$) for the 15 datasets of Physionet for various kernel sizes. The hue of the markers is proportional to the kernel size. The four inner plots with the yellow background on the right of each subplot, depict the corresponding kernel for the kernel size that achieved the best $\bar{\varphi}$. The datasets are arranged with an increasing $\bar{\varphi}$ of the Peak activation function.

TABLE I
KERNEL SIZES m WITH THE BEST $\bar{\varphi}$ FOR EACH SPARSE ACTIVATIONS ON PHYSIONET DATABASES

Datasets	Identity				Max-Activation				Max-Pool indices				Peaks			
	m	CR^{-1}	$\tilde{\mathcal{L}}$	$\bar{\varphi}$	m	CR^{-1}	$\tilde{\mathcal{L}}$	$\bar{\varphi}$	m	CR^{-1}	$\tilde{\mathcal{L}}$	$\bar{\varphi}$	m	CR^{-1}	$\tilde{\mathcal{L}}$	$\bar{\varphi}$
apnea-ecg	59	0.88	0.36	0.62	66	0.10	0.38	0.24	71	0.10	0.30	0.20	75	0.10	0.31	0.20
bpssrat	39	1.04	0.34	0.69	16	0.14	0.61	0.38	19	0.12	0.40	0.26	16	0.13	0.36	0.24
voiced	41	1.00	0.28	0.64	44	0.09	0.54	0.32	76	0.10	0.45	0.28	67	0.10	0.41	0.25
slpdb	12	0.73	0.53	0.63	35	0.09	0.64	0.37	164	0.18	0.53	0.36	131	0.14	0.44	0.29
sufhsdb	39	1.05	0.25	0.65	40	0.09	0.79	0.44	50	0.09	0.39	0.24	56	0.08	0.51	0.30
wrist	77	0.73	0.61	0.67	37	0.09	0.74	0.42	158	0.17	0.46	0.31	159	0.17	0.42	0.30
mitdb	66	0.78	0.50	0.64	35	0.09	0.62	0.36	187	0.20	0.51	0.35	55	0.08	0.59	0.33
bidmc	5	0.82	0.51	0.66	31	0.10	0.86	0.48	10	0.10	0.59	0.34	95	0.10	0.61	0.35
prcp	4	1.00	0.52	0.76	25	0.10	0.81	0.46	25	0.07	0.67	0.37	39	0.06	0.69	0.37
noneeg	3	0.91	0.57	0.74	52	0.09	0.89	0.49	30	0.06	0.73	0.40	29	0.05	0.71	0.38
ctu-uhb-ctgdb	5	0.50	0.58	0.54	18	0.13	0.78	0.45	47	0.08	0.73	0.40	43	0.06	0.72	0.39
cebsdb	3	0.95	0.51	0.73	115	0.13	0.83	0.48	11	0.10	0.60	0.35	73	0.08	0.71	0.39
shhpsgdb	2	0.82	0.62	0.72	27	0.10	0.89	0.50	12	0.13	0.73	0.43	19	0.06	0.76	0.41
emgdb	3	0.96	0.61	0.78	20	0.12	0.84	0.48	20	0.09	0.78	0.43	8	0.07	0.76	0.42
drivedb	1	0.59	0.72	0.66	10	0.21	0.63	0.42	28	0.09	0.75	0.42	32	0.07	0.77	0.42

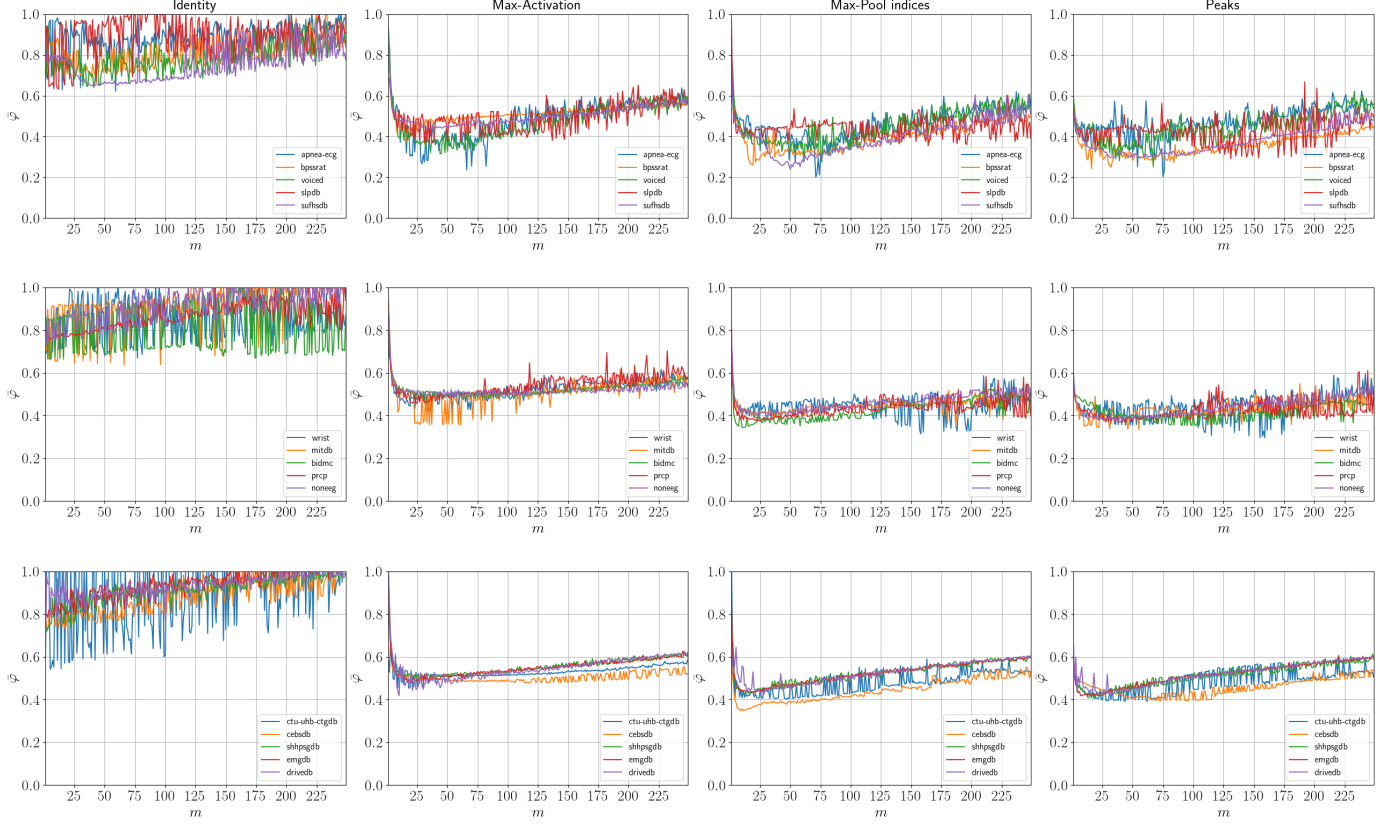


Fig. 4. $\bar{\varphi}$ vs. m . Columns correspond to different activation functions while rows correspond to five out of 15 of the Physionet datasets (split in three rows for easing the visualizations).

TABLE II
SANs WITH SUPERVISED STACKED CNN FOR UCI-EPILEPSY CLASSIFICATION

m	Identity				Max-Activation				Max-Pool indices				Peaks			
	CR^{-1}	$\tilde{\mathcal{L}}$	$\bar{\varphi}$	Acc(%)	CR^{-1}	$\tilde{\mathcal{L}}$	$\bar{\varphi}$	Acc(%)	CR^{-1}	$\tilde{\mathcal{L}}$	$\bar{\varphi}$	Acc(%)	CR^{-1}	$\tilde{\mathcal{L}}$	$\bar{\varphi}$	Acc(%)
15	2.16	0.07	1.12	90.8	0.42	0.79	0.60	74.1	0.33	0.50	0.41	70.8	0.26	0.49	0.38	74.7
16	2.18	0.02	1.10	91.2	0.39	0.78	0.58	75.6	0.34	0.48	0.41	70.0	0.27	0.50	0.39	71.2
17	2.20	0.02	1.11	91.3	0.42	0.78	0.60	74.9	0.34	0.49	0.41	69.9	0.28	0.50	0.39	37.8
18	2.20	0.04	1.12	89.7	0.40	0.79	0.60	72.7	0.34	0.51	0.42	73.4	0.28	0.50	0.39	75.4
19	2.21	0.07	1.14	89.8	0.42	0.78	0.60	75.6	0.34	0.49	0.41	74.9	0.29	0.50	0.40	73.0
20	2.22	0.04	1.13	86.3	0.40	0.78	0.59	75.1	0.40	0.51	0.45	79.3	0.34	0.49	0.41	72.3
21	2.24	0.02	1.13	89.1	0.42	0.77	0.59	75.8	0.36	0.49	0.43	74.3	0.35	0.47	0.41	81.3
22	2.25	0.03	1.14	87.8	0.43	0.77	0.60	77.3	0.37	0.49	0.43	76.7	0.32	0.50	0.41	73.9

TABLE III
SAN WITH SUPERVISED STACKED FNN ON MNIST

m	Identity				Max-Activation				Max-Pool indices				Peaks			
	CR^{-1}	$\tilde{\mathcal{L}}$	$\bar{\varphi}$	Acc(%)	CR^{-1}	$\tilde{\mathcal{L}}$	$\bar{\varphi}$	Acc(%)	CR^{-1}	$\tilde{\mathcal{L}}$	$\bar{\varphi}$	Acc(%)	CR^{-1}	$\tilde{\mathcal{L}}$	$\bar{\varphi}$	Acc(%)
1	0.00	1.00	0.50	11.3	0.58	0.00	0.29	91.9	0.58	0.00	0.29	91.0	0.04	0.89	0.47	81.7
2	0.63	0.00	0.31	91.6	0.57	0.01	0.29	91.0	0.48	0.61	0.55	93.3	0.04	0.88	0.46	82.9
3	0.75	0.00	0.38	90.7	0.63	0.26	0.44	89.6	0.29	0.51	0.40	92.6	0.03	0.66	0.34	77.3
4	0.01	1.00	0.51	11.3	0.20	0.44	0.32	85.8	0.21	0.59	0.40	91.6	0.04	0.69	0.37	77.2
5	0.01	1.00	0.51	11.3	0.20	0.54	0.37	86.7	0.09	0.66	0.37	90.0	0.01	1.00	0.51	11.3
6	0.69	0.03	0.36	91.2	0.08	0.71	0.39	73.4	0.07	0.70	0.38	88.5	0.03	0.74	0.38	64.3

the DNNs and in some cases without sacrificing significant accuracy.

Regarding their architecture, a difference of SANs with

traditional autoencoders is that they contain shared weights instead of tied weights, where the weights are transposed

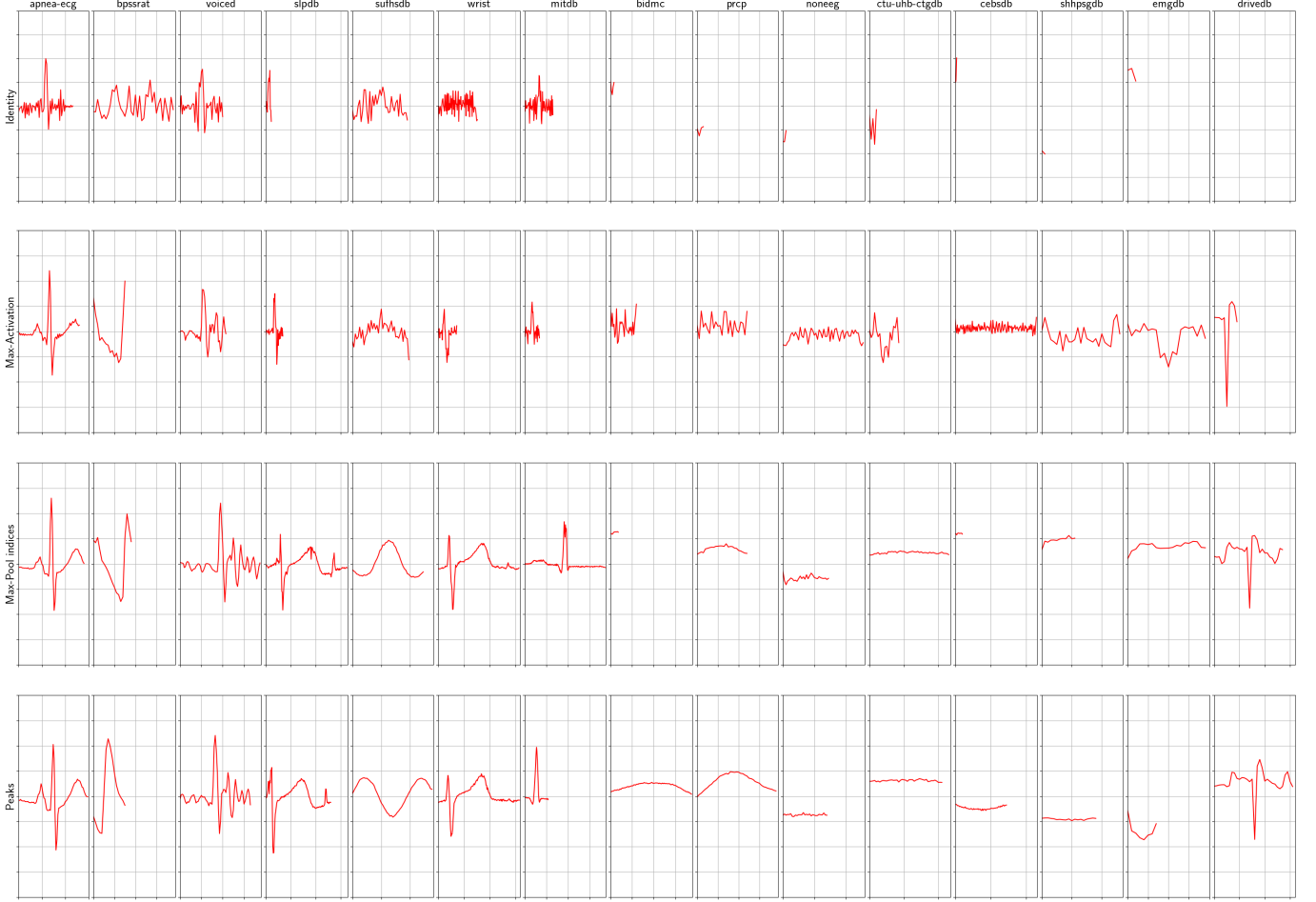


Fig. 5. Visualization of the learned kernels for each sparse activation function (row) and for each Physionet database (column).

during decoding. The latter were initially used in autoencoders to resemble Principal Component Analysis when the activation functions are linear. Moreover, an adding gate is placed before the output of SANs to sum up the individual reconstructions from each kernel.

φ could be seen as an alternative formalization of Occam’s razor [35] to Solomonov’s theory of inductive inference [36] but with a deterministic interpretation instead of a probabilistic one. The cost of the description of the data could be seen as proportional to the number of weights and the number of non-zero activations, while the quality of the description is proportional to the reconstruction loss. The φ metric is also related to the rate-distortion theory [37], in which the maximum distortion is defined according to human perception, which however inevitably introduces a bias. There is also relation with the Compressed Sensing area [38] in which the sparsity of the data is exploited allowing us to reconstruct it with fewer samples than the Nyquist-Shannon theorem requires. Olshausen et al. [39] presented an objective function that considers subjective measures of sparseness of the activation maps, however in this work we use the direct measure of compression ratio. Previous work by [40] have used a weighted combination of the number of neurons, percentage

root-mean-squared difference and a correlation coefficient for the optimization function of a FNN as a metric but without taking consideration the number of non-zero activations.

A limitation of SANs is the use of amplitude-only variable kernels, which are not sufficient for more complex data and also do not fully utilize the compressibility of the data. A possible solution would be using a grid sampler [41] on the kernel allowing it to learn more general transformations (such as scale) than simple amplitude variability. However, additional kernel properties should be chosen in correspondence with the φ metric i.e. the model should compress more with decreased reconstruction loss.

VI. CONCLUSIONS AND FUTURE WORK

In this paper we defined SANs which have minimal structure and learn to compress data without losing important information. We also defined the φ metric to evaluate how well do SANs trade-off reconstruction loss with compression. Using Physionet datasets and MNIST we demonstrated that SANs are able to create high quality representations with interpretable kernels.

The minimal structure of SANs makes it easy to use for feature extraction, clustering and time-series forecasting. Other future work on SANs include:

- Applying cosine annealing to the peak distance in order to increase the degree of freedom of the kernels.
- Imposing the minimum peak distance along all similarity matrices for multiple kernels, thus making kernels compete for territory.
- Applying dropout at the activations in order to correct weights that have overshoot, especially when they are initialized with high values. However, the effect of dropout on SANs would generally be negative since SANs have much less weights than DNNs thus need less regularization.
- Using SANs with dynamically created kernels that might be able to learn multimodal data from variable sources (e.g. from ECG to respiratory) without destroying previous learned weights.

ACKNOWLEDGMENT

This work was supported by the European Union's Horizon 2020 research and innovation programme under Grant agreement 769574. We gratefully acknowledge the support of NVIDIA with the donation of the Titan X Pascal GPU used for this research.

REFERENCES

- [1] Y. LeCun, Y. Bengio, and G. Hinton, "Deep learning," *nature*, vol. 521, no. 7553, p. 436, 2015.
- [2] D. E. Rumelhart, G. E. Hinton, and R. J. Williams, "Learning representations by back-propagating errors," *nature*, vol. 323, no. 6088, p. 533, 1986.
- [3] D. P. Kingma and J. Ba, "Adam: A method for stochastic optimization," *arXiv preprint arXiv:1412.6980*, 2014.
- [4] A. Krizhevsky, I. Sutskever, and G. E. Hinton, "Imagenet classification with deep convolutional neural networks," in *Advances in neural information processing systems*, 2012, pp. 1097–1105.
- [5] A. Graves, A.-r. Mohamed, and G. Hinton, "Speech recognition with deep recurrent neural networks," in *2013 IEEE international conference on acoustics, speech and signal processing*. IEEE, 2013, pp. 6645–6649.
- [6] C. Szegedy, V. Vanhoucke, S. Ioffe, J. Shlens, and Z. Wojna, "Rethinking the inception architecture for computer vision," in *Proceedings of the IEEE conference on computer vision and pattern recognition*, 2016, pp. 2818–2826.
- [7] K. Simonyan and A. Zisserman, "Very deep convolutional networks for large-scale image recognition," *arXiv preprint arXiv:1409.1556*, 2014.
- [8] K. He, X. Zhang, S. Ren, and J. Sun, "Deep residual learning for image recognition," in *Proceedings of the IEEE conference on computer vision and pattern recognition*, 2016, pp. 770–778.
- [9] C. Zhang, S. Bengio, M. Hardt, B. Recht, and O. Vinyals, "Understanding deep learning requires rethinking generalization," *arXiv preprint arXiv:1611.03530*, 2016.
- [10] J. Frankle and M. Carbin, "The lottery ticket hypothesis: Finding sparse, trainable neural networks," *arXiv preprint arXiv:1803.03635*, 2018.
- [11] A. Aghasi, A. Abdi, N. Nguyen, and J. Romberg, "Net-trim: Convex pruning of deep neural networks with performance guarantee," in *Advances in Neural Information Processing Systems*, 2017, pp. 3177–3186.
- [12] J. Lin, Y. Rao, J. Lu, and J. Zhou, "Runtime neural pruning," in *Advances in Neural Information Processing Systems*, 2017, pp. 2181–2191.
- [13] S. B. Laughlin and T. J. Sejnowski, "Communication in neuronal networks," *Science*, vol. 301, no. 5641, pp. 1870–1874, 2003.
- [14] D. P. Kingma and M. Welling, "Auto-encoding variational bayes," *arXiv preprint arXiv:1312.6114*, 2013.
- [15] Y. Bengio, P. Simard, P. Frasconi *et al.*, "Learning long-term dependencies with gradient descent is difficult," *IEEE transactions on neural networks*, vol. 5, no. 2, pp. 157–166, 1994.
- [16] X. Glorot, A. Bordes, and Y. Bengio, "Deep sparse rectifier neural networks," in *Proceedings of the fourteenth international conference on artificial intelligence and statistics*, 2011, pp. 315–323.
- [17] V. Nair and G. E. Hinton, "Rectified linear units improve restricted boltzmann machines," in *Proceedings of the 27th international conference on machine learning (ICML-10)*, 2010, pp. 807–814.
- [18] K. He, X. Zhang, S. Ren, and J. Sun, "Delving deep into rectifiers: Surpassing human-level performance on imagenet classification," in *Proceedings of the IEEE international conference on computer vision*, 2015, pp. 1026–1034.
- [19] I. J. Goodfellow, D. Warde-Farley, M. Mirza, A. Courville, and Y. Bengio, "Maxout networks," *arXiv preprint arXiv:1302.4389*, 2013.
- [20] A. Makhzani and B. Frey, "K-sparse autoencoders," *arXiv preprint arXiv:1312.5663*, 2013.
- [21] P. Bush and T. Sejnowski, "Inhibition synchronizes sparsely connected cortical neurons within and between columns in realistic network models," *Journal of computational neuroscience*, vol. 3, no. 2, pp. 91–110, 1996.
- [22] Y. Bengio, D.-H. Lee, J. Bornschein, T. Mesnard, and Z. Lin, "Towards biologically plausible deep learning," *arXiv preprint arXiv:1502.04156*, 2015.
- [23] M. Rehn, "A network that uses few active neurones to code visual input," *Science*, vol. 301, pp. 1870–1874.
- [24] T. Heiberg, B. Kriener, T. Tetzlaff, G. T. Einevoll, and H. E. Plesser, "Firing-rate models for neurons with a broad repertoire of spiking behaviors," *Journal of computational neuroscience*, vol. 45, no. 2, pp. 103–132, 2018.
- [25] P. Bizopoulos and D. Koutsouris, "Deep learning in cardiology," *IEEE reviews in biomedical engineering*, vol. 12, pp. 168–193, 2019.
- [26] K. Simonyan, A. Vedaldi, and A. Zisserman, "Deep inside convolutional networks: Visualising image classification models and saliency maps," *arXiv preprint arXiv:1312.6034*, 2013.
- [27] M. D. Zeiler and R. Fergus, "Visualizing and understanding convolutional networks," in *European conference on computer vision*. Springer, 2014, pp. 818–833.
- [28] S. Bach, A. Binder, G. Montavon, F. Klauschen, K.-R. Müller, and W. Samek, "On pixel-wise explanations for non-linear classifier decisions by layer-wise relevance propagation," *PloS one*, vol. 10, no. 7, p. e0130140, 2015.
- [29] M. T. Ribeiro, S. Singh, and C. Guestrin, "Why should i trust you?: Explaining the predictions of any classifier," in *Proceedings of the 22nd ACM SIGKDD international conference on knowledge discovery and data mining*. ACM, 2016, pp. 1135–1144.
- [30] L. Blier and Y. Ollivier, "The description length of deep learning models," in *Advances in Neural Information Processing Systems*, 2018, pp. 2216–2226.
- [31] A. Paszke, S. Gross, S. Chintala, G. Chanan, E. Yang, Z. DeVito, Z. Lin, A. Desmaison, L. Antiga, and A. Lerer, "Automatic differentiation in pytorch," 2017.
- [32] A. L. Goldberger, L. A. Amaral, L. Glass, J. M. Hausdorff, P. C. Ivanov, R. G. Mark, J. E. Mietus, G. B. Moody, C.-K. Peng, and H. E. Stanley, "Physiobank, physiotoolkit, and physionet: components of a new research resource for complex physiologic signals," *Circulation*, vol. 101, no. 23, pp. e215–e220, 2000.
- [33] R. G. Andrzejak, K. Lehnertz, F. Mormann, C. Rieke, P. David, and C. E. Elger, "Indications of nonlinear deterministic and finite-dimensional structures in time series of brain electrical activity: Dependence on recording region and brain state," *Physical Review E*, vol. 64, no. 6, p. 061907, 2001.
- [34] Y. LeCun, L. Bottou, Y. Bengio, P. Haffner *et al.*, "Gradient-based learning applied to document recognition," *Proceedings of the IEEE*, vol. 86, no. 11, pp. 2278–2324, 1998.
- [35] A. N. Sokolov, "Occams razor as a formal basis for a physical theory," *Foundations of Physics Letters*, vol. 15, no. 2, pp. 107–135, 2002.
- [36] R. J. Solomonoff, "A formal theory of inductive inference. part i," *Information and control*, vol. 7, no. 1, pp. 1–22, 1964.
- [37] T. Burger, "Rate distortion theory," 1971.
- [38] D. L. Donoho *et al.*, "Compressed sensing," *IEEE Transactions on information theory*, vol. 52, no. 4, pp. 1289–1306, 2006.
- [39] B. A. Olshausen and D. J. Field, "Emergence of simple-cell receptive field properties by learning a sparse code for natural images," *Nature*, vol. 381, no. 6583, p. 607, 1996.
- [40] B. Zhang, J. Zhao, X. Chen, and J. Wu, "Ecg data compression using a neural network model based on multi-objective optimization," *PloS one*, vol. 12, no. 10, p. e0182500, 2017.
- [41] M. Jaderberg, K. Simonyan, A. Zisserman *et al.*, "Spatial transformer networks," in *Advances in neural information processing systems*, 2015, pp. 2017–2025.